



Evaluation of ANFIS and LR models for seismic rockfalls' susceptibility mapping: a case study of Firooz Abad-Kojour, Iran, Earthquake (2004)

Vahid Bagheri¹ · Ali Uromeihy¹ · Seyed Mahmood Fatemi Aghda²

Received: 17 February 2018 / Accepted: 1 December 2018 / Published online: 11 December 2018
© Springer-Verlag GmbH Germany, part of Springer Nature 2018

Abstract

Seismic rockfall is one of the prevalent geohazards that cause huge losses in the earthquake-stricken areas. In the present research, a model is developed to map susceptibility (occurrence probability) of seismic rockfalls in a regional scale using Logistic Regression (LR) and Adaptive Neuro-Fuzzy Inference System (ANFIS) techniques. In this research, Firooz Abad-Kojour earthquake of 2004 was introduced as the benchmark and the model base. The susceptible zones predicted by LR and ANFIS methods were compared with the database (distribution map) of seismic rockfalls, by which the results revealed a good overlapping between the susceptible zones predicted by the ANFIS and the field observation of rockfalls triggered by this earthquake. Besides, for the statistical evaluation of results obtained by LR and ANFIS models, the verification parameters with high accuracy such as density ratio (Dr), quality sum (Qs), and receiver-operating characteristic curve (ROC) were used. By analyzing the susceptibility maps and considering the Qs index obtained by LR (21.04184) and ANFIS (26.75592), it could be found that the Qs of ANFIS is higher than that of LR. Moreover, based on the obtained value of the area under the curve (AUC) from LR (0.972) and ANFIS (0.984) methods, ANFIS provided a higher accuracy in zonation and susceptibility mapping of rockfalls triggered by Firooz Abad-Kojour earthquake of 2004 compared to the LR method.

Keywords Seismic rockfalls · Hazard zonation · Firooz Abad-Kojour · Susceptibility mapping · Logistic regression · Adaptive neuro-fuzzy inference system

Introduction

Landslide, earthquake, flood, and volcano are among the prevalent natural disasters that annually impose huge financial and life losses to humans. By population growth and increasing construction in landslide-prone areas, global statistics of landslide-based casualties are continuously rising. According to the World Atlas of Natural Hazards, landslides are the most abundant and widespread natural disasters on Earth. In this regard, the susceptibility and damage maps of landslides can be considered as a basis for crisis management of those regions. The maps also are important tools

for engineers, geologist, planners, and decision-makers to select suitable places for agriculture, construction, and other developmental activities (Ercanoglu and Gokceoglu 2002).

Rockfalls are the downward motion of rock fragments involving free falling, bouncing, and rolling, which, depending on the changes in the topographic profile, two or more forms of rockfalls may be seen. Rockfall is a very common event that occurs in mountainous slopes, coastal cliffs, volcanoes, riverside, and trenches. Although most of the rockfalls occur in the remote area, they can be a serious threat to residential area and transportation lines (Hung et al. 1999; Chau et al. 2003; Corominas et al. 2005). The high hazard of rockfalls is mainly due to their dynamic behavior, the velocity of the block motion (30–100 km/h), and the difficulty of predicting the source of their occurrence. The high velocity and sudden occurrence of rockfalls make it different from other slope instabilities. The affected area by rockfalls can be identified through the existence of cracks and crashed blocks on the surface of the slope. It is worth pointing out that detection of rockfalls in the area is possible in the case of less vegetation. In areas susceptible to rockfall hazard,

✉ Ali Uromeihy
uromeiea@modares.ac.ir

Vahid Bagheri
vahid.bagheri@modares.ac.ir

¹ Department of Geology, Faculty of Basic Sciences, Tarbiat Modares University, Tehran 14115-111, Iran

² Department of Applied Geology, Faculty of Geological Sciences, Kharazmi University, Tehran, Iran

the occurrence of multiple rockfalls results in the formation of debris deposits in the heel of the slope (Corominas et al. 2017).

The unpredictable nature of most of the rockfalls has been a concern for authorities and decision-makers. Although the dimensions of rockfalls are limited, they are a very fast event with high kinetic energy that makes enormous damage. Turner and Jayaprakash (2012) presented a complete list of rockfalls, which showed that even rocks with less volume could be resulted in a significant destruction and blockage of roads, especially in railway lines. The recent research (Petley 2012) showed that the most landslide and rockfall-induced losses were observed in most of the less developed countries due to the lack of research and suitable resources.

In general, the trigger factor in rockfalls is related to the existence of previous shear or tensile fracture along the discontinuity, which led to the detachment and creation of potentially unstable blocks from the slope (Valagussa et al. 2014b). Gosar (2017) classified the rockfalls into five classes based on volume and frequency (Table 1). The blocks can be triggered by many factors including seismic movements of the earth, rainfall, increasing the pore pressure in the rock mass, melting–freezing cycle, chemical decomposition, advanced weathering of the rock mass, root wedging caused by winds, and progressive decomposition of rock mass (Varnes 1978). The rockfalls originate from cliffs with different size, lithology, and structure. Rockfalls and other kinds of landslides are secondary effects of large earthquakes. Therefore, rockfall hazard zonation is an important issue for planning the land use, especially in seismic regions with steep slopes.

Given that no research has been conducted on zonation and mapping the susceptibility of seismic rockfalls using intelligent methods (such as ANFIS), the present research was carried out to implement the ANFIS and LR methods in the area stricken by Firooz Abad-Kojour earthquake of 2004, evaluate and select the optimum model with high accuracy in prediction, mapping the susceptibility of seismic rockfalls, and apply this method to predict probability of rockfall events induced by future earthquakes. In the present research, Geographic Information System (ArcGIS), PCI Gematica (Landsat Satellite Image Processing), SPSS

22 (to implement LR), and MATLAB 2014 (Neuro-fuzzy network implementation environment) were used.

Materials and methods

Study area description

Geographical setting of the study area

Topographically, the study area, which was stricken by Firooz Abad-Kojour earthquake of 2004, is one of the highlands of Alborz Mountain. Damavand Peak with a height of 5671 meters—the highest peak of Iran—is located in this area. The average height of the area is over than 2000 m (A.S.L). The existence of deep and steep valleys and long crests are the main characteristics of this area in Alborz. Based on the classification of plain and mountainous regions, more than 80% of the earthquake-stricken parts of the study area are located in a mountainous region. The plain and low-lying regions of the study area are limited to small parts of the valleys bottom and the southern margin of the Caspian Sea. The selected stricken areas are located in longitude of 51°00′–52°00′ N and latitude of 36°00′–36°30′E (Fig. 1). Firooz Abad-Kojour earthquake of 2004 resulted in casualties and financial losses from the south of Chalus, Firooz Abad, Kojour valley, Marzan Abad, Kelardasht, and Chalus Road to the western parts of Roudbar Alamut district of Qazvin province, Iran (Zare 2004).

Geological conditions of the study area

The study area is located in the central part of the Alborz Mountains. Alborz mountain range was created by severe Alpine orogenic movement. Today, these tectonic movements are observed in forms of folds, faults, and thrusts. Although the general trend of folds and their structure affected by Alborz Mountain and it is East–West, there are many irregularities in this trend. In Stratigraphic view, the main part of the study area is covered by Karaj Formation, which is often pyroclastic and includes a wide range of tuff, agglomerate, shale, sandstone, and volcanic and intrusive rocks. It followed by sandy-shale Shemshak Formation. In addition to Karaj and Shemshak formations, the rock units related to Precambrian until the end of the third era are outcropped in a different part of the area, and the multiple fractures and folds caused by tectonic movement are the common point of the rock units. In the eastern and central parts, the calcareous deposits and pyroclastic rocks are outcropped, respectively. From central part to the western part of the study area, the Neogene marl and conglomerates deposits are covered the dominant part of the area (Amini Hosseyni et al. 2004; Mahdaviifar 2006). The geological map of study

Table 1 Distribution of rockfalls according to their size

| Size of rockfall | Estimated volume (m ³) | Number |
|------------------|------------------------------------|--------|
| Very small | 10 ² | 53 |
| Small | 10 ³ | 13 |
| Medium | 10 ⁴ | 6 |
| Large | 10 ⁵ | 4 |
| Very large | > 10 ⁶ | 2 |



Affected Area by the Firooz Abad-Kojour Earthquake

Fig. 1 Geographical setting map of the region affected by Firooz Abad-Kojour earthquake of 2004

is shown in Fig. 2. Besides, lithological description of the geological terms used in Fig. 2 is presented in Table 2.

Characteristics of the Firooz Abad-Kojour earthquake of 2004 and its causative fault

In 28th May 2004, the Firooz Abad-Kojour earthquake of 2004 shook the northwest of central Alborz and part of western Alborz at 17:08:46 h (local time). The earthquake with magnitudes of 6.2 (M_w) and focal depth of 18 km was felt in south of Chalus, Kojour valley, and Marzan Abad area, which along with casualties and financial loss from Firooz Abad (Kojour), Marzan Abad, Kelardasht, and Chalus road (Mazandaran province) areas to western parts of Roudbar Alamut district of Qazvin province. According to the recorded strong motion data in the main shock and

locating the earthquake focal point, the epicenter was located at 36.35°N, 51.35°E. Based on the report of Harvard University website, the earthquake focal mechanism was introduced as compressive with a small strike-slip component. Given the location of earthquake focus, seismic epicenter zone, and faults in the area, the north fault of Alborz was introduced as a causative fault (Fig. 3) (Zare 2004).

Based on the damages in the seismic epicenter, field observation of Baladeh to Kojour Valley, observing the residential area in Chalus valley, and due to the focus of the rockfalls in the range of Hezarcham to Siyahbishe on the Chalus Road, it seems that, in epicenter zone and in the area of rockfalls in Chalus road, the intensity of the earthquake was in the VII+ and VIII+ (on the EMS scale), respectively. On the other hand, the expansion of the iso-seismical line in the epicentral zone showed the earthquake intensity of

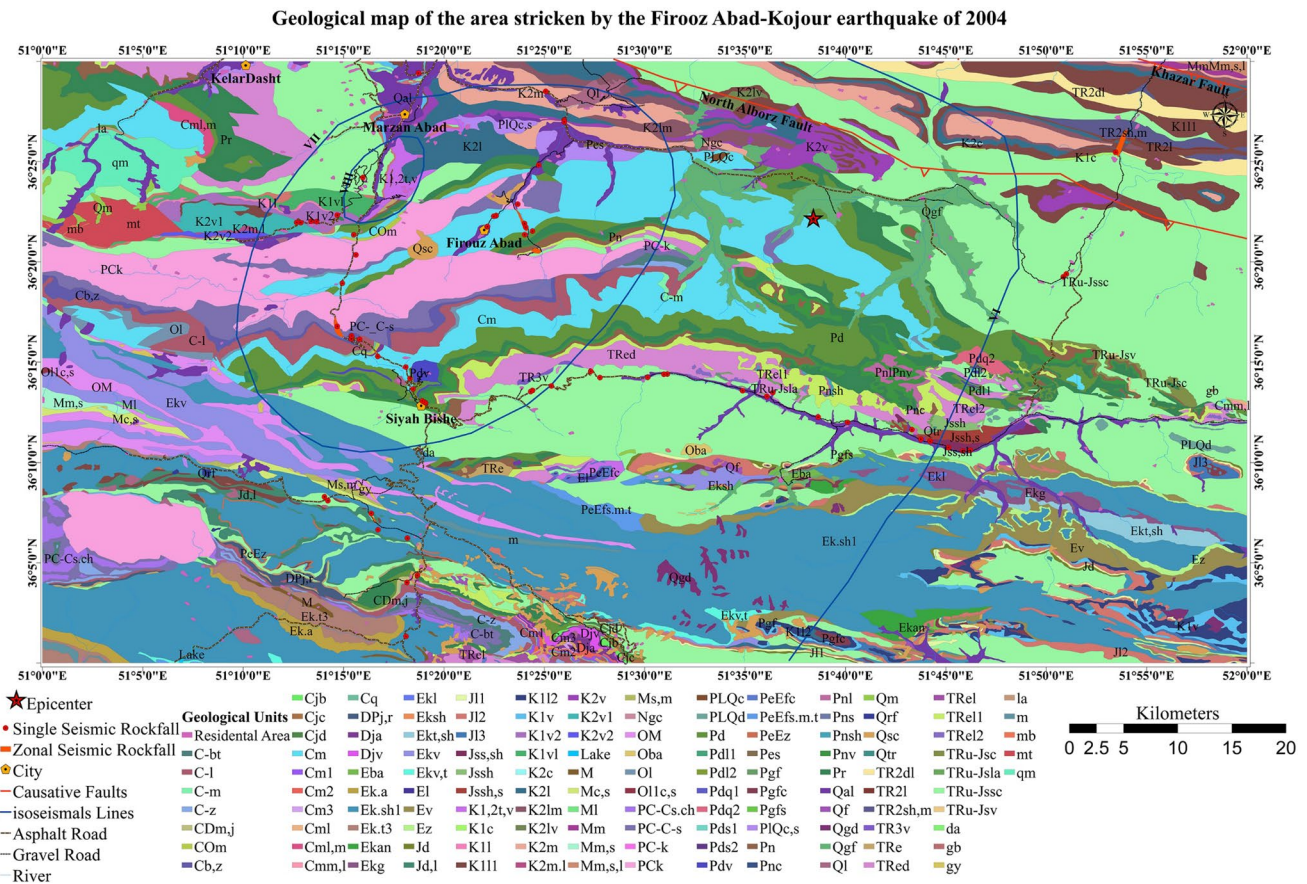


Fig. 2 Geological map of the area stricken by the Firooz Abad-Kojour earthquake of 2004

north and North West of Tehran which was VI (Fig. 3) (Zare 2004).

Rockfalls induced by the Firooz Abad-Kojour earthquake of 2004 in the study area

Firooz Abad-Kojour earthquake of 2004 due to the topographic conduction and existence of Mountains and steep areas resulted in numerous slope instability in a large part of the Central Alborz. The instabilities were expanded in the area of 12,000 km² (around the earthquake epicenter) in forms of rockfalls and small and large slides. In the study area, about 74 falls and falling zone were recorded (Fig. 4). The furthest distance from the falling event to the earthquake epicenter is about 101 km, which occurred within 27 km of the Qazvin road to Moallem Kalayeh. This distance was in agreement with the distance of seismic landslides presented by Keefer (1984). The rockfalls are concentrated in the central, western, southern, and southwest areas of the iso-intensity line (Chalus road, Baladeh, and adjacent areas of Sama village, Firooz Abad, Manjir, etc.). In geological point of view, these areas consist of Precambrian (sandstone, slits of Kahar formation) and Cambrian formations (sandstone and

shale). The presence of weak rocks and rough topography has greatly increased the potential for landslides occurred in the region. The landslides commonly occur in the length of the steep valley and more dispersed in areas with a mild topography. The most abundant type of seismic landslides is shallow and severely disrupted falls, and rocks and debris slide that has spread throughout the region. Coherent slump and block slides occur in rocks with higher strength. The highest number of seismic rockfalls occurred in the range of Chalus road (between the HaftBaradar and Hezarcham) and the linking road of Sama village to Manjir in Sanj Mountain. In some parts, more than 40% of slopes were affected by the earthquake (Amini Hosseyni et al. 2004). The depth of landslides varies from several decimeters to several meters and affects the dry and unconsolidated materials. The volume of these instabilities varies from a fraction of cubic meters to several thousand cubic meters. Within the Chalus Road, the highest casualties and damage are caused by seismic rockfalls. Besides, the similar rockfalls were observed in the range of Sama Village to Manjir (close to the epicenter) and the roads around it. Seismic rockfalls resulted in many financial losses and casualties in villages, one can name Anarak, Firooz Abad, Sama, Manjir, Larak, etc.

Table 2 Lithological description of the geological terms used in Fig. 2

| Geological units | Descriptions |
|------------------|---|
| Qal | Loose alluvium in the river channels |
| K1v | Volcanics including basalt and spilite |
| | Residential area |
| PIQc,s | Conglomerate, sandstone, mudstone intercalations |
| TRed | Massive dolomite |
| Pn | Cherty limestone, marly limestone, marly, and sandy shales |
| Pr | Gray, thick-bedded to massive limestone and dolomite |
| Ql | Landslide, rock stream |
| Cm | Black limestone, dolomitic limestone, marl intercalations |
| Cml,m | Limestone, marl, siltstone |
| K2m | Marl, calcareous marl, marly limestone |
| la | Larvikitic border facies (Nepheline syenite) |
| Pes | Calcareous sandstone, sandy limestone |
| qm | Akapol quartz monzonite |
| TRe | Undivided Elika formation |
| K1v1 | Dark colored basic and intermediate to basic volcanics, pyroclastics, tuff, conglomerate |
| K1v2 | Alkali basalt, spilitic basalt, conglomerate, tuff braccia, tuffs, lithic tuff |
| mt | Metamorphic Cretaceous volcanic sequences Green schists, hornfels, schist, marbles |
| K1l | Limestone (Berriasian—Valanginian) |
| K2v1 | Dark colored volcanic rocks, conglomerate, tuff breccia, and pyroclastics |
| COm | Undivided mila formation |
| mb | Marble, marmorized limestone |
| K2v2 | Trachyandesitic basalt, tuff breccia, pyroclastics, tuffite |
| K2m.1 | Marly limestone, limestone (Cenomanian—Coniacian) |
| Cb,z | Undivided Barut and Zagun Formation |
| Ekv | Trachyandesite, trachy basalt, basanite, andesite, agglomerate, tuffs, pyroclastics |
| Cq | White quartzite, quartzitic sandstone (formerly top quartzite) |
| O1 | Sandstone, shale, trilobite bearing limestone and marl, quartzite, Dolomite |
| Dja | Sandstone, shale, limestone, marl phosphatic layers |
| Qf | Young and old alluvial fans, fanglomerate |
| M | Undivided Miocene deposits including silty marl, siltstone, conglomerate, gypsum |
| J12 | Cream, thick-bedded to massive limestone, dolomitic limestone and dolomite, partly cherty |
| Pdv | Basic volcanics, tuff, pyroclastics, sandstone |
| O11c,s | Red conglomerate, sandstone |
| Mm,s | Silty marl, sandstone, mudstone, siltstone gypsum |
| Ek.sh1 | Lower shale member calcareous and siliceous shales, tuffite, pyroclastics, dacitic |
| Ml | Limestone |
| Mc,s | Conglomerate, sandstone |
| gy | Gypsum |
| Ek.t3 | Upper tuff Member Tuffs, pyroclastics, calcareous shale, mudstone, sandstone |
| da | Rhyodacite—rhyolite (Paleogene—Oligocene) |
| Qm | Moraines (glacial deposits) |
| K1,2t,v | Undivided cretaceous tuffs, siltstone and volcanics |
| K2l | Globotruncana limestone, marly limestone |
| Ms,m | Calcareous sandstone, silty marl |
| TR3v | Olivine basalt, andesitic basalt, pyroclastics |
| E1 | Limestone, marly limestone |
| PCk | Slaty shale, sandstone, siltstone, dolomite, quartzite |
| OM | Siltstone, marl, sandstone, conglomerate, limestone, gypsum |
| Jd,1 | Undivided Dalichai and lar formations |

Table 2 (continued)

| Geological units | Descriptions |
|------------------|---|
| PeEz | Alveolina—nummulitic limestone |
| Qrf | Rock fall |
| DPj,r | Undivided Jeirud and Ruteh formations |
| Ek.a | Asara shale member calcareous—tuffaceous shale, siltstone, sandstone |
| CDm,j | Undivided Mila and Jeirud formations |
| Djv | Basaltic—andesitic lava flows |
| Cm3 | Pink—white Trilobite bearing limestone (third member) |
| Cm2 | Dark colored Trilobite bearing dolomitic limestone (second member) |
| Cm1 | Dark colored massive dolomite and fissile yellow marl (first member) |
| Cjc | Light grey massive dolomitic limestone |
| Cjd | Black oolitic and intraclastic limestone |
| PC-Cs.ch | Dark colored shale and siltstone |
| Cjb | Black limestone, clayey marl intercalations |
| m | Monzonite, monzosyenite (paleogene—probably oligocene) |
| Lake | Lake of Amir Kabir dam |
| TRel | Thick-bedded to massive limestone |
| PeEfc | Thick-bedded to massive polygenetic dark colored conglomerate, sandstone |
| PeEfs.m.t | Sandstone, shale, marl, tuff, siltstone, conglomerate, limestone |
| Mm,s,l | Marl, sandstone silty marl and minor limestone |
| Mm | Marl, sandstone, and calcareous sandstone with a lot of shell fragments |
| K111 | Cream to white, thick-bedded to massive limestone and a conglomerate horizon at the base |
| K2lv | Yellowish gray, thick-bedded to massive limestone and volcanics including basalt |
| K2c | Red well-sorted, thick-bedded, polymictic conglomerate |
| TR2l | Violet, thick-bedded to massive limestone |
| TR2sh,m | Shale and marl with intercalations of silty sandstone containing marine fauna |
| K1c | Gray-to-red thick-bedded conglomerate |
| Ngc | Poorly consolidated, poorly sorted, polymictic conglomerate |
| K2lm | Gray, yellow, light green, limestone, argillaceous limestone, and marl |
| PLQc | Slightly consolidated conglomerate |
| TR2dl | Light gray-to-black, well-bedded dolomite |
| K2v | Volcanics including basalt, spilite, and andesite–basalt |
| Pnv | Black, dark green volcanics including basalt and spilite |
| TRel1 | Light gray, green, and red laminated to thin-bedded argillaceous limestone |
| PC-k | Shale, micaceous sandstone and minor dolomite |
| PC-C-s | Gray, thick-bedded to massive dolomite partly crystallized (Soltanieh dolomite) |
| C-bt | Red shale, siltstone and sandstone with intercalations of dolomite |
| C-z | Red, siltstone, shale and sandstone |
| C-l | Red, medium to thick-bedded, cross-bedded arkosic-to-subarkosic sandstone |
| C-m | Gray dolomite, limestone, marl, sandstone and shale |
| Pdq2 | White, gray, thick-bedded quartz arenite |
| Pnl | Dark gray, black, thick-bedded to massive fossiliferous limestone |
| Pd | Quartz arenite, limestone, and volcanics |
| Pdl2 | Cream, yellow, and gray fusulinid limestone |
| Pds2 | Red and gray sandstone over-laine by alternation of limestone and sandstone |
| Pdl1 | Gray, thick-bedded, oncolytic, fossiliferous, reefal limestone containing coral and fusulinid |
| Pds1 | Red and gray sandstone with intercalations of pebbly sandstone |
| Pdq1 | White, gray quartz arenite red, thick-to-medium bedded sandstone and pebbly sandstone |
| TRu-Jsv | Volcanics including basalt, andesite, and dacite |
| Pnsh | Black calcareous and gypsiferous shale with abundant brachiopod |
| TRu-Jssc | Gray, well-consolidated, well-rounded pebbly sandstone |

Table 2 (continued)

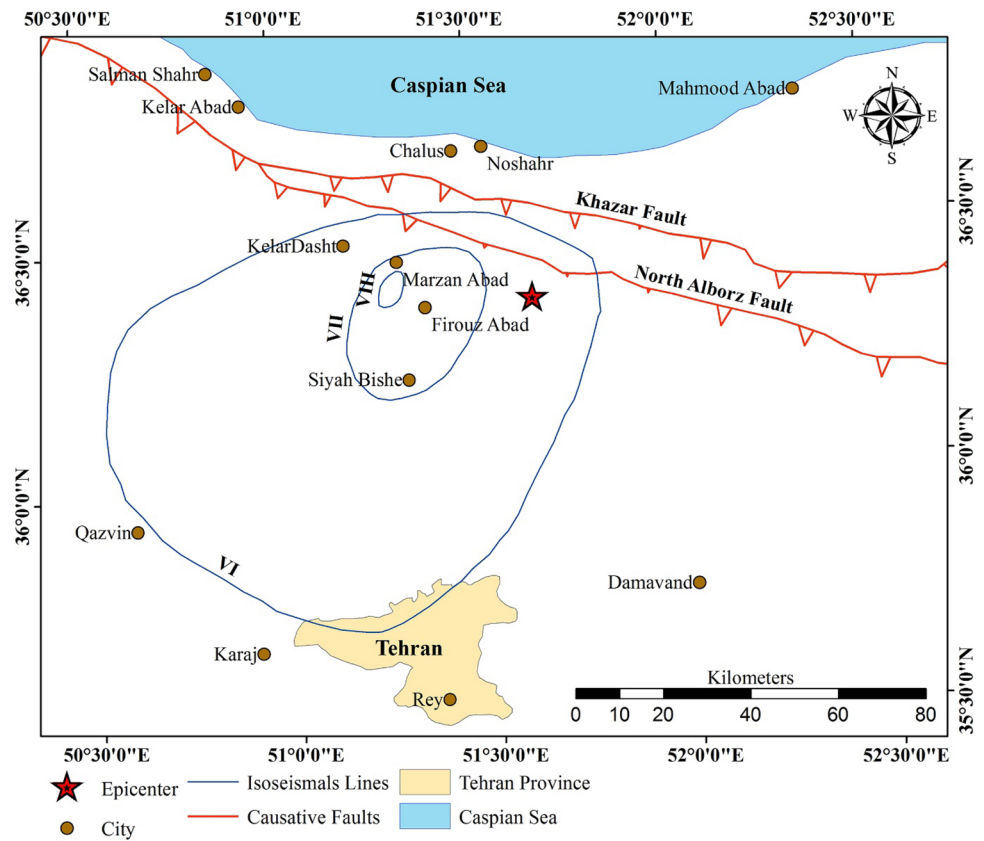
| Geological units | Descriptions |
|------------------|---|
| gb | Gabbro (post-rheato-liassic) |
| Jssh | Black, carbonaceous shale |
| Pns | Gray, red coarse grained quartz-rich sandstone |
| Cml | Gray-to-black, thin-bedded to massive argillaceous limestone |
| Cmm,l | Gray-to-black, platy, fossiliferous argillaceous limestone and marl |
| PLQd | Dacitic doms and veins |
| Pnc | Red, well-bedded, well-sorted, well-consolidated, polymictic conglomerate |
| TRu-Jsc | Thick-bedded to massive quartzose conglomerate |
| TRel2 | Cream, brownish, thick-bedded, limestone and dolomitic limestone |
| Jssh,s | Black shale and dark gray micaceous sandstone |
| TRu-Jsla | Dark red laterite and lateritic shale (paleosol) |
| Jss,sh | Gray, micaceous sandstone, argillaceous sandstone, and shale locally with coal seams |
| Eba | Basalt |
| Jl3 | Gray, thick-bedded to massive dolomite and dolomitic limestone |
| Qsc | Scree slope deposits |
| Ekg | Gypsum |
| Ekan | Andesite |
| Ekl | Limestone, argillaceous, gray |
| Ev | Volcanics including agglomerate, volcanic breccia, basalt, and spilitic |
| Qgf | Glaciofluvial deposits |
| Qgd | Glaciogenic deposits |
| Eksh | Black and grey shale, partly calcareous |
| Ekt,sh | Green tuff, tuffaceous shale, and green-to-dark grey shale |
| Oba | Olivine basalt |
| Qtr | Travertine |
| Jd | Dark green, ammonite bearing argillaceous limestone and marl |
| Pgfs | Dark red, coarse grained conglomeratic sandstone and shale |
| K112 | Cream to gray, thick-bedded orbitolinid and rudist bearing limestone |
| Ekv,t | Volcanics including andesite, andesite-basalt tuff, thin-to-thick-bedded, green and grey |
| Pgf | Red coarse grained conglomerate and sandstone |
| Jl1 | Greenish gray-to-light gray, thin-to-medium bedded, ammonite bearing argillaceous limestone |
| Ez | Thin-to-thick-bedded nummulitic limestone, partly argillaceous and arenaceous |
| Pgfc | Red, thick-bedded to massive conglomerate |

The Firooz Abad-Kojour Earthquake of 2004 led to 41 life losses and huge financial loss such as destruction of buildings and vehicles. The highest rate of casualties was related to the falling of huge rocky blocks and hit cars passing through Chalou to Tehran road (Amini Hosseini et al. 2004; Mahdaviifar 2006). The samples related to Firooz Abad-Kojour seismic rockfalls are presented in Figs. 5a–d and 6a, b. Moreover, Table 3 presents geological and morphological properties of some dominant discontinuities effective in rockfall events induced by Firooz Abad-Kojour of 2004 recorded during the field survey.

Background of the research

Estimating the rockfalls hazard for zonation requires the determination of the event probability (Cancelli and Crosta 1993; Corominas et al. 2005; Jaboyedoff et al. 2005; Straub and Schubert 2008; Agliardi et al. 2009). For seismic rockfalls, the occurrence probability is affected by event probability of earthquakes with different intensity. For other types of landslides, expanded studies were performed on the relationship between earthquake and landslide occurrence through experimental (Keefer 1984;

Fig. 3 Iso-intensity map of the Firooz Abad-Kojour earthquake of 2004



Distribution map of Rockfalls induced by the Firooz Abad-Kojour earthquake of 2004 within the study area

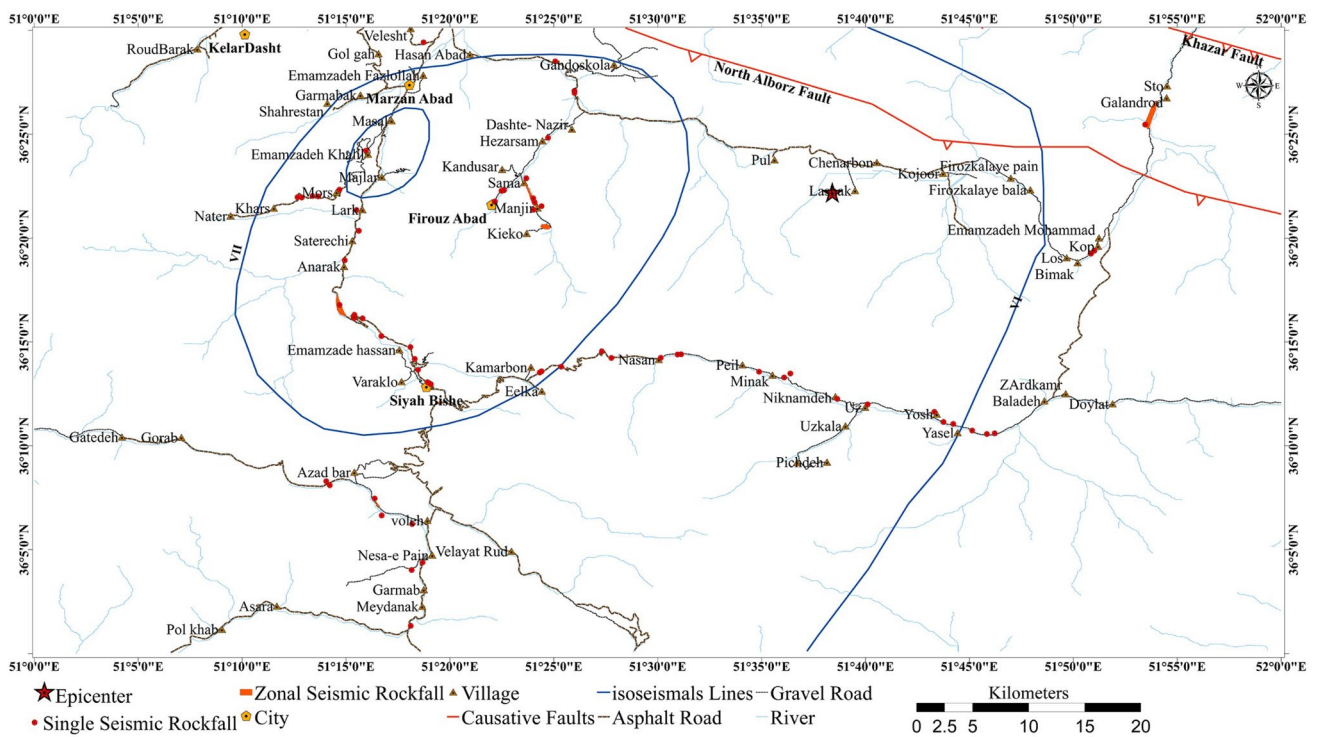


Fig. 4 Distribution map of Rockfalls induced by the Firooz Abad-Kojour earthquake of 2004 within the study area

Fig. 5 Rockfalls triggered by the Firooz Abad-Kojour earthquake of 2004 within the study area: **a** falling rocks on the Baladeh road, 19 km from Haraz to Baladeh; **b** rockfall and blockage of road from Kojour to Baladeh; **c** rockfalls on the link road of Sama village to Manjir in Sanj Mountain; **d** farms stricken by rockfalls around of Sama village; consider the mud trace resulting from rockfalls on walls

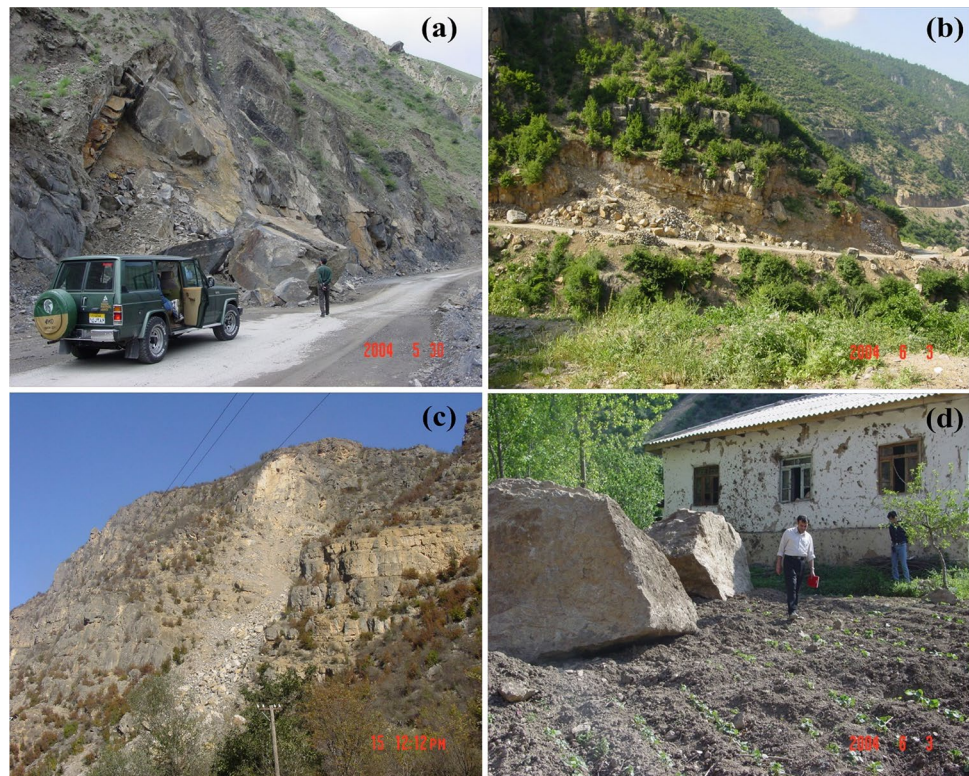


Fig. 6 Rockfalls triggered by the Firooz Abad-Kojour earthquake of 2004 within the study area: **a** falling zone in Chalus road, 12 km from Baladeh three ways to Chalus; **b** blockage of some parts of Chalus road due to rockfalls in 14 Km of Baladeh three ways to Karaj



Rodriguez et al. 1999; Lee et al. 2008; Miles and Keefer 2009a, b), physical, or numerical methods (Jibson et al. 2000; Wasowski and Del Gaudio 2000; Capolongo et al. 2002; Del Gaudio et al. 2003; Del Gaudio and Wasowski 2004; Uchida et al. 2006; Peng et al. 2009; Rapolla et al. 2010; Motamedi and Liang 2013). In fact, less number of research (Marzorati et al. 2002; Valagussa et al. 2014a, b; Lari et al. 2014; Massey et al. 2015; Mahdavifar et al. 2016) was conducted on seismic rockfalls hazard zonation and susceptibility mapping. In these studies, the seismic rockfall probability was predicted by hierarchical methods and statistical methods such as information value and logistic regression (LR) generally. The above-mentioned

methods, however, are not efficient in areas that the rockfall probability is affected by the earthquake.

Required information layers for LR and ANFIS methods

The region stricken by the Firooz Abad-Kojour earthquake of 2004 has a 4983 km² area. In this research, various information layers with a pixel size of 10 m × 10 m were prepared. The determination of cell size is based on the minimum precision of all causative factors to guarantee the quality of output maps and avoid misleading results. Unit categorization of the study area was performed using the

Table 3 Geological and morphological properties of some dominant discontinuities effective in rockfall events induced by Firooz Abad-Kojour of 2004

| No. | Longitude | Latitude | Average sea level (m) | Lithology | Average slope angle | Aspect | Spacing (cm) | Filling | Maximum opening (cm) | Discontinuity condition | Weathering rate |
|-----|------------|------------|-----------------------|---------------------|---------------------|--------|--------------|---------------|----------------------|-------------------------|----------------------|
| 1 | 51.8475059 | 36.3208962 | 1820 | Andesite | 35 | 85 | 200 | None | 3 | Rough | Slightly weathered |
| 2 | 51.85013 | 36.3233 | 1786 | Shale and sandstone | 35 | 170 | 100 | Silt and Marl | 10 | Slightly rough | Moderately weathered |
| 3 | 51.7702512 | 36.1766757 | 2142 | Sandstone | 50 | 165 | 40 | None | 3 | Rough | Slightly weathered |
| 4 | 51.7639934 | 36.1761681 | 2131 | Sandstone | 55 | 170 | 90 | None | 2 | Rough | Slightly weathered |
| 5 | 51.7370274 | 36.1842212 | 2146 | Sandstone | 48 | 160 | 60 | None | 3 | Rough | Slightly weathered |
| 6 | 51.7218478 | 36.1939084 | 2143 | Sandstone | 45 | 145 | 50 | None | 2 | Rough | Slightly weathered |
| 7 | 51.66842 | 36.19988 | 2280 | Sandstone | 35 | 210 | 40 | None | 3 | Rough | Slightly weathered |
| 8 | 51.6440376 | 36.2042851 | 2346 | Shale and sandstone | 35 | 65 | 50 | None | 2 | Slightly rough | Moderately weathered |
| 9 | 51.6014083 | 36.2215124 | 2349 | Sandstone | 85 | 150 | 40 | None | 4 | Rough | Slightly weathered |
| 10 | 51.51596 | 36.23994 | 2582 | Sandstone | 47 | 10 | 30 | Marl | 2 | Slightly rough | Slightly weathered |
| 11 | 51.50247 | 36.23731 | 2629 | Sandstone | 55 | 30 | 20 | Marl | 5 | Slightly rough | Slightly weathered |
| 12 | 51.46288 | 36.23716 | 2855 | Sandstone | 35 | 185 | 100 | None | 2 | Slightly rough | Slightly weathered |
| 13 | 51.45523 | 36.2424 | 2907 | Shale | 35 | 125 | 8 | Marl | 2 | Smooth | Moderately weathered |
| 14 | 51.42256 | 36.23019 | 2701 | Shale | 45 | 115 | 40 | Marl | 3 | Smooth | Moderately weathered |
| 15 | 51.40685 | 36.22645 | 2615 | Shale | 37 | 125 | 100 | Marl | 3 | Smooth | Moderately weathered |
| 16 | 51.40538 | 36.22551 | 2594 | Shale | 45 | 195 | 70 | None | 3 | Smooth | Moderately weathered |
| 17 | 51.2729593 | 36.1244147 | 3464 | Tuff and sandstone | 35 | 180 | 150 | None | 5 | Slightly rough | Moderately weathered |
| 18 | 51.2753081 | 36.1193899 | 3050 | Shale and sandstone | 35 | 265 | 120 | None | 3 | Slightly rough | Moderately weathered |

ArcGIS environment. Through this process, the spatial position of each pixel is fixed with respect to all information layers. Therefore, for a given pixel with fixed spatial coordinates, the predefined information and values are recorded. Finally, each pixel contains data from all information layers as well as the presence or lack of seismic rockfall.

There are much affecting and triggering factors used in the literature for landslide hazard zonation. The most important triggering factors are earthquake and rainfall, and most important affecting factors are slope angle and ground strength (Yin and Yan 1988; Budimir et al. 2015). Furthermore, the importance of affecting factors changes for different landslide types. For example, soil moisture is not an important factor in rockfall occurrence, while it is one of the most important factors in soil slump occurrence. In this research, seismic rockfalls' susceptibility mapping and hazard zonation are investigated, and hence, important factors for rockfall occurrence are chosen for analysis.

The initial information layers used in this research are distribution map of the rockfalls induced by the Firooz Abad-Kojour earthquake of 2004, aspect, distance from the river, distance from the road, ground strength class, hypocentral distance, shake intensity (MMI), slope angle, and slope height in the study area. Using the distribution map of the rockfalls triggered by the Firooz Abad-Kojour earthquake of 2004, the other information layers were classified.

Ground strength class information layer is established based on the description and information provided by Keefer (2000) about the relationship between the qualitative characteristics of slope materials (lithology) and concentration of seismic rockfalls. The ground strength class is related to the lithology unit ranking based on their susceptibility to seismic rockfalls. To prepare this information layer, the 1:50,000 geological maps of the area stricken by the Firooz Abad-Kojour earthquake of 2004 were used, and then, these maps were elaborated using the field visit data and 1:20,000 aerial photos. For each lithology unit in the study area, a ground strength class value was assigned in the range of 1–5 and accuracy of 0.5 (Fatemi Aghda and Bagheri 2015). These values are proportional to the concentration of seismic rockfalls calculated for each lithology. This information layer is a representative of ground conditions, material properties such as shear strength, and rock mass joints. The lower ground strength class values suggest the weaker and higher susceptibility of the ground-to-seismic landslide occurrence (Miles and Keefer 2007).

To prepare shake intensity data layer, first, moment magnitude of earthquake (M_w), the distance of each unit from epicenter (R), and Eq. 1 (Mahdaviifar et al. 2007) were used to provide Arias Intensity (Arias 1970) map (with pixel size of 10 m × 10 m). Then, using Eq. 2 (Wilson 1993), shake intensity map was based on the MMI (Fatemi Aghda and Bagheri 2015):

$$\log I_a = -3.880 + 0.810M - \log R - 0.002R, \quad (1)$$

where I_a is Arias Intensity in m/s, M is the moment magnitude, and R is the source-to-site distance in km.

Source-to-site distance (R), which is defined as the shortest distance between accelerometer stations and the fault rupture plan at the earthquake focal depth (h) is obtained by $R = \sqrt{r^2 + h^2}$:

$$\log(I_a) = 0.527 I_{\text{MMI}} - 3.816, \quad (2)$$

where I_{MMI} is the shake intensity in MMI.

Seismic rockfalls' susceptibility mapping using LR method

A bivariate LR is a multivariate statistical method, which is generalized by linear models and introduced by Cox (1958). Besides, it forms a mathematical model to predicts the probability of occurrence of an event in the determined location. This model evaluates the absence or existence of a dependent variable in connection with the independent variables (Garsia et al. 2008). When the dependent variable is dichotomous (1 and 0), bivariate LR is the best choice for statistical analysis. In comparison with linear regression method, LR method has three advantages. First, in contrast to linear regression, variables in LR do not require to have a normal distribution. Second, independent variables in the LR may be continuously or categorized, or their combination. Third, LR method needs fewer assumptions (Chauhan et al. 2010). LR method is a quantitative method, which determines the effect of each independent variable on dependent variable quantitatively through coefficient (Lee and Sambath 2006; Garsia et al. 2008; Nefeslioglu et al. 2008; Dashti Marvily 2008; Yilmaz 2009). In bivariate LR model, the coefficient of independent variables (effective and trigger parameters) is estimated using maximum-likelihood method. The formula of LR is presented in the following equation:

$$Y = \text{Logit}(p) = \ln \left(\frac{p}{1-p} \right) = \beta_0 + \beta_1 X_1 + \beta_2 X_2 + \dots + \beta_n X_n, \quad (3)$$

where Y is dependent variable, X_1, X_2, \dots, X_n is independent variables, Logit is probability logarithm or the natural amount of probability logarithm, p is probability of dependent variable (Y), $\left(\frac{p}{1-p} \right)$ is likelihood or disagreement ratio,

β_0 is constant coefficient, and $\beta_1, \beta_2, \dots, \beta_n$ are coefficients of independent variables.

The results indicate the relationship between the seismic rockfalls and their causative factors. In the LR method, the dependent input variable should be dichotomous, i.e., it only contains data coded as 1 (rockfalls) or 0 (non-rockfalls). The LR method does not directly indicate the susceptibility and, however, provide an inference to show the susceptibility rate

using probability (Ayalew and Yamagishi 2005; Lee and Sambath 2006; Garsia-Rodríguez et al. 2008; Nefeslioglu et al. 2008).

Since the application of LR method is to identify the best model for creating a relationship between the trigger and effective parameters of seismic rockfalls with dichotomous dependent variable (coded with 1 and 0 for occurrence of rockfall and non-occurrence of rockfall), in the present research, to develop the LR method, the random sampling was performed in non-falling parts of the study area, provided that the stable and unstable points did not coincide (74 falling and 74 non-falling points; code 1 and 0, respectively). Table 4 not only provides a summary of the role of each

variable in the model but also indicates that which variables remain in the model after performing LR. Table 4 is the most important tool in interpretation related to significance (Wald) and effective rate of each independent variable on dependent one ($\text{Exp}(\beta)$). It should be noted that Wald statistic was employed to find which independent variables have a significant effect on the dependent variable. Besides, to determine the effective rate of each independent variable on dependent one, odds ratio statistics were used. As shown in Eq. 4, the value of Wald test is calculated by the comparison of maximum-likelihood estimation of each coefficient (β) with standard estimated error (SE) of each coefficient. Interpretation of the Wald statistics values is performed by

Table 4 Influence coefficients (β), Wald values, and $\text{Exp}(\beta)$ of trigger and effective parameters of Firooz Abad-Kojour seismic rockfalls (2004) using LR based on backward conditional rule in SPSS software

| Variables in the equation | | | | | | |
|---------------------------|--------------|-----------|-----------------|-------------------|-------------------|-----------------------|
| Steps | Factors | β^a | SE ^b | Wald ^c | Sig. ^d | $\text{Exp}(\beta)^e$ |
| Step 1 ^a | Aspect | -0.501 | 0.365 | 1.882 | 0.170 | 0.606 |
| | Slope | 2.210 | 0.710 | 9.675 | 0.002 | 9.112 |
| | River | 1.281 | 0.586 | 4.787 | 0.029 | 3.602 |
| | Road | 0.994 | 0.338 | 8.668 | 0.003 | 2.701 |
| | MMI | 2.790 | 2.080 | 1.800 | 0.180 | 16.284 |
| | R | 1.246 | 1.177 | 1.120 | 0.290 | 3.475 |
| | Ground | 0.893 | 0.419 | 4.545 | 0.033 | 2.441 |
| | Slope height | -1.078 | 0.693 | 2.423 | 0.120 | 0.340 |
| Step 2 ^a | Constant | -18.739 | 5.522 | 11.515 | 0.001 | 0.000 |
| | Aspect | -0.437 | 0.354 | 1.527 | 0.217 | 0.646 |
| | Slope | 2.031 | 0.644 | 9.951 | 0.002 | 7.624 |
| | River | 1.224 | 0.554 | 4.886 | 0.027 | 3.402 |
| | Road | 1.017 | 0.323 | 9.902 | 0.002 | 2.766 |
| | MMI | 4.611 | 1.312 | 12.360 | 0.000 | 100.604 |
| | Ground | 0.866 | 0.417 | 4.314 | 0.038 | 2.377 |
| | Slope height | -1.025 | 0.688 | 2.219 | 0.136 | 0.359 |
| Step 3 ^a | Constant | -17.937 | 5.025 | 12.740 | 0.000 | 0.000 |
| | Slope | 1.787 | 0.553 | 10.441 | 0.001 | 5.972 |
| | River | 1.143 | 0.508 | 5.057 | 0.025 | 3.135 |
| | Road | 1.058 | 0.310 | 11.609 | 0.001 | 2.880 |
| | MMI | 4.221 | 1.149 | 13.506 | 0.000 | 68.107 |
| | Ground | 0.865 | 0.384 | 5.088 | 0.024 | 2.375 |
| | Slope height | -0.909 | 0.631 | 2.079 | 0.149 | 0.403 |
| | Constant | -17.996 | 4.613 | 15.218 | 0.000 | 0.000 |
| Step 4 ^a | Slope | 1.439 | 0.461 | 9.743 | 0.002 | 4.217 |
| | River | 0.983 | 0.434 | 5.136 | 0.023 | 2.673 |
| | Road | 0.984 | 0.289 | 11.562 | 0.001 | 2.675 |
| | MMI | 3.585 | 0.927 | 14.960 | 0.000 | 36.037 |
| | Ground | 0.736 | 0.332 | 4.898 | 0.027 | 2.087 |
| | Constant | -16.600 | 3.856 | 18.535 | 0.000 | 0.000 |

^aFactor coefficient

^bStandard error

^cWald test value

^dSignature level

^eOdds ratio

evaluating the significance level (Sig.) of each variable. Accordingly, if the significance level of each variable is less than 0.05, the existence of this variable in the model is beneficial and has a significant effect. The sign of independent variable coefficient (β) reveals the direct effect or reverse effect of the variable on the dependent variable (Chauhan et al. 2010). The coefficients obtained by LR method, the Wald values, and related Exp (β) are presented in Table 4.

$$Wald = \left(\frac{\beta}{SE} \right)^2 \tag{4}$$

Considering the results of fourth step in Table 4, the independent variables, including shake intensity, slope angle, ground strength class, distance from the road, and distance from the river, are able to predict the changes in the dependent variables of occurrence or non-occurrence of seismic rockfall. Besides, their prediction ability is significant at <0.05. On the other hand, among the remaining significant independent variables, shake intensity and ground strength class, respectively, have the highest and lowest abilities to susceptibility mapping of Firooz Abad-Kojour seismic rockfalls (2004). Based on the fourth step of Table 4, the

independent variables of shake intensity, slope angle, ground strength class, distance from the road, and distance from the river, have a positive and direct relationship with the dependent variable of occurrence or non-occurrence of rockfall triggered by Firooz Abad-Kojour earthquake of 2004.

In the present research, to weight the parameters and related classes to each parameter, the LR analysis of SPSS software and fuzzy logic of ArcGIS software were, respectively, employed. After performing four steps of LR analysis based on “backward condition” rule in the SPSS software (Table 4) and determining the suitable weights for selected parameters (shake intensity, slope angle, ground strength class, distance from the road, and distance from the river), first, the information layers were fuzzified in the ArcGIS software to weight the sub-criteria of those parameter. Then, the weights obtained from Step 4 were multiplied and overlapped with corresponding parameters, such that to prepare the map of seismic rockfall susceptibility (Fig. 7). In ArcGIS software, the seismic rockfall susceptibility zonation map is classified into five classes of “very low hazard”, “low hazard”, “moderate hazard”, “high hazard”, and “very high hazard” due to the natural breaks (Swets 1988; Bednarik et al. 2010; Constantin et al. 2011; Pourghasemi et al. 2012a,

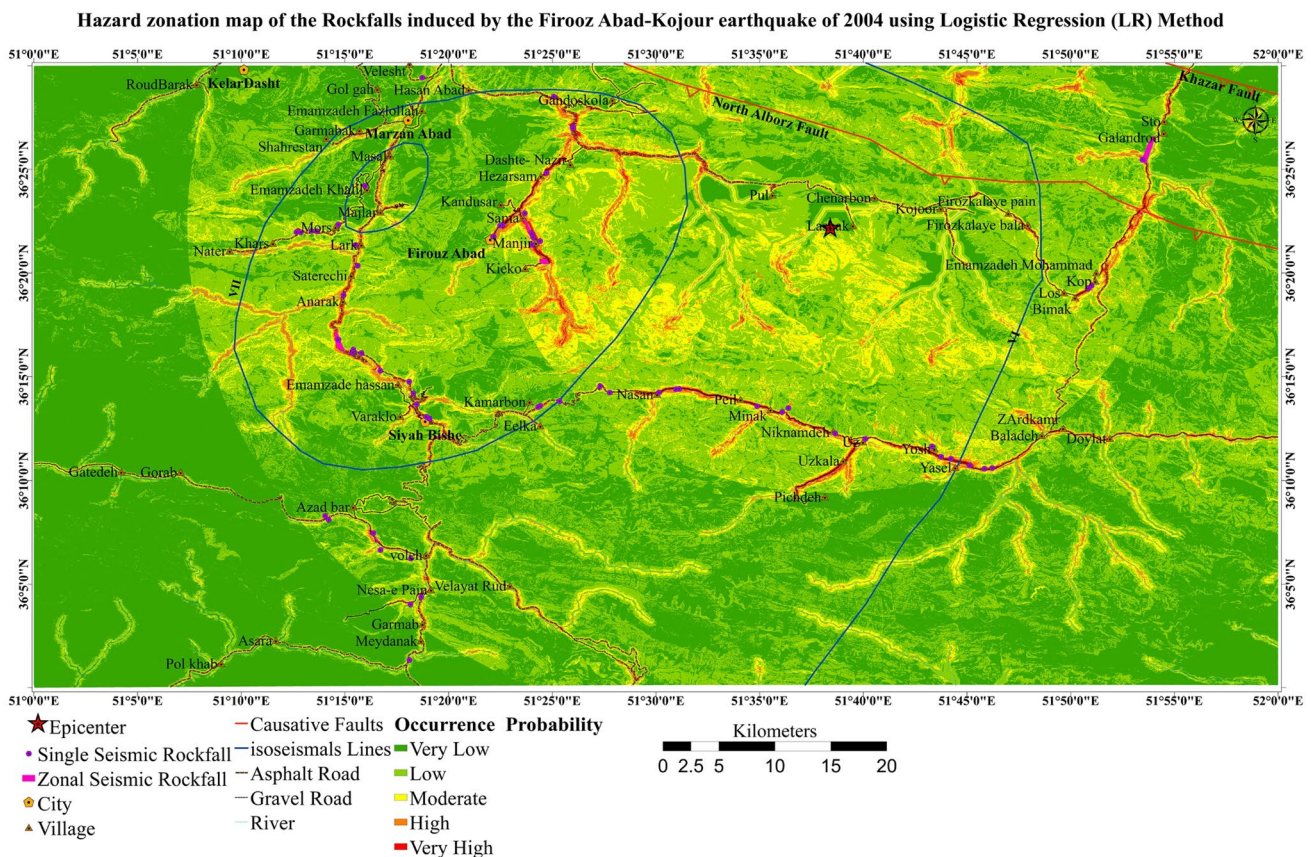


Fig. 7 Hazard zonation map of the rockfalls induced by the Firooz Abad-Kojour earthquake of 2004 using logistic regression (LR) method

2013). By this way, the boundary between the susceptibility levels of seismic rockfalls was determined by the abrupt change in the corresponding histogram curve.

As shown in Fig. 7, the maximum area is related to “very low hazard” and “low hazard” classes (shown in dark green and green regions, respectively). In general, the percentage of susceptible area for seismic rockfalls was reduced by increasing the hazard in related zones. As can be seen, the majority of rockfalls triggered by Firooz Abad-Kojour earthquake of 2004 is placed in “high hazard” to “very high hazard” zones.

Besides, all parts close to linking roads, rivers, the parts with a steep slope, the areas around earthquake epicenter, and parts with consisting of low-strength geological formation show a “high”-to-“very high” rockfall susceptibility level. Since rockfalls mostly occur in scraps and steep areas and considering the rough morphology of streams and road-side features, the high concentration of rockfalls within the area stricken by Firooz Abad-Kojour earthquake of 2004 along these points is logical (Fig. 7). Therefore, it can be concluded the desirable accuracy of LR analysis in preparation of hazard zonation map for the rockfalls induced by the Firooz Abad-Kojour earthquake of 2004.

Seismic rockfalls’ susceptibility mapping using ANFIS method

In most problems of the real world, by increasing the number of variables, determination of linguistic rule is being difficult. Therefore, due to the impossibility of complete defining the mentioned rules, learning algorithms are used to synthesize the fuzzy model, which is called neuro-fuzzy modeling (Jang 1993). Although the fuzzy models are able to show the complicated process using concepts and rules of “if-then”, they are not able to learn. Besides, in the case of a high number of variables in the description of a problem, the choice of membership function and suitable “if-then” rule is difficult in the fuzzy model and the adjustment step of the fuzzy model will be unlimited. This problem can be solved using artificial neural learning algorithm such as optimization methods (Backpropagation algorithm) (Yesilnacar 2005; Polat and Güneş 2006). In this method, learning algorithm automatically chooses the suitable parameter for membership function in the fuzzy model. Although the neural networks are able to learn, they cannot explain the complexity of the mentioned system. Therefore, adaptive neuro-fuzzy inference system (ANFIS) method is used, which is a developed fuzzy model and trained by learning algorithm of neural network theory (Polat and Güneş 2006). The other capability of ANFIS, which almost overcomes the disadvantages of the fuzzy model, is its self-learning feature. ANFIS creates a fuzzy inference system (FIS) using input and output data sets. The parameters of the membership function of

ANFIS are adjusted through back propagation algorithm or hybrid learning principle (combination of back propagation algorithm with least squares method) (Ying and Pan 2008; Oh and Pradhan 2011). The adjustment operations allow the fuzzy system to learn own structure from the data set.

ANFIS structure with two inputs is shown in Fig. 8. Each input has two membership functions; consequently, this structure has four principles. Besides, ANFIS model is a five-layered structure and each of them is described here.

The first layer: in this layer, the membership degree of each input to corresponding fuzzy set is calculated (Eqs. 5 and 6):

$$O_i^1 = \mu A_i(x), \tag{5}$$

$$O_i^1 = \mu B_i(y), \tag{6}$$

where x and y are input variables of i node, A and B are a linguistic label, and $\mu A_i(x)$ and $\mu B_i(x)$ are fuzzy membership function associated with this node. Parameters are referred to as “premise parameters”.

Second layer: every node in this layer is a fixed-node labeled Π . The output of each node is a multiplication of all the input signals to the node, which equivalents to “if” part of the fuzzy rule (Eq. 7):

$$O_i^2 = w_i = \mu A_i(x) \times \mu B_i(y), \quad i = 1, 2, \tag{7}$$

where w_i is weight or firing strength of each fuzzy principle of “if-then” rule.

Third layer: every node in this layer is a fixed-node labeled N . The nodes of this layer calculate the normalized output of second layer (Eq. 8):

$$O_i^3 = \bar{w}_i = \frac{w_i}{w_1 + w_2}, \quad i = 1, 2, \tag{8}$$

where O_i^3 is the weight of normalized firing strength of the third layer.

The fourth layer: the output of this layer is the multiplication of previous layer output by a first-order polynomial (first-order Sugeno model) (Eq. 9):

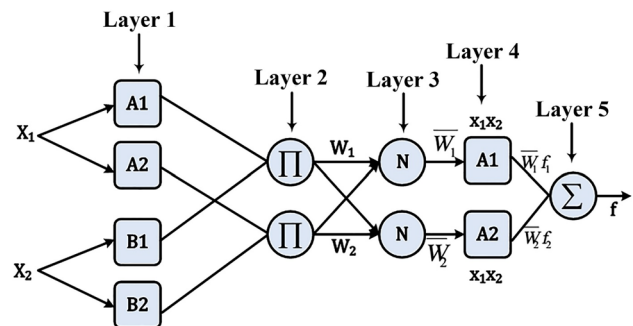


Fig. 8 ANFIS with two inputs and one output (Sugeno 1985)

$$O_i^4 = \bar{w}_i f_i = \bar{w}_i(p_i x + q_i y + r_i), \tag{9}$$

where \bar{w}_i is normalized firing strength of third layer, and p_i , q_i , and r_i are the parameter set of i nodes. These are referred to as consequent parameters, which can be adjusted during the training process.

Fifth layer: the single node in this layer is labeled Σ , which computes the overall output as the summation of all incoming signals (Eq. 10):

$$O_i^5 = \text{overalloutput} = \sum \bar{w}_i f_i = \frac{\sum w_i f_i}{\sum w_i}, i = 1, 2, \tag{10}$$

where O_i^5 is the i th node output of the fifth layer (Wang and Elhag 2008; Bui et al. 2012).

The final output of the ANFIS is the mean weighted outputs of all rules (Eq. 11):

$$y(k) = \frac{\sum_{i=1}^l \{ \text{rule}_i(k) [r_{1,i}(k) + p_{1,i}(k)x + q_{1,i}(k)y] \}}{\sum_{i=1}^l \text{rule}_i(k)}. \tag{11}$$

To implement ANFIS for Firooz Abad-Kojour seismic rockfalls' susceptibility mapping, MATLAB software was employed. It should be noted that, to determine the efficiency of ANFIS and modeling, data were normalized before entering to the software. Besides, to design ANFIS, five selected input parameters (shake intensity, distance from the road, slope angle, distance from the river, and ground strength class) were used based on the LR method (the fourth step of Table 4). After normalization and preparing data, the data of study area were divided into two groups of "train" and "test" data. In the present research, 70% and 30% of data from each hazard zone, respectively, were used as train and test data. The next step was ANFIS design. There are several methods to design ANFIS such as "Grid Partition" and "Subtractive

Clustering". In the present research, "Subtractive Clustering" method was used. In this method, not only there is no need to determine the type and number of the membership function, but also the designed algorithm by network determines the number of the membership function. It means that the number of the membership function is determined based on the frequency and distribution of information. In addition, in this method, the type of input and output membership functions is considered "Gaussian" and "Linear" by default, respectively. The advantage of "Subtractive Clustering" method is that the data mining of data obtain from study area and determination of whether the designed network needs adding complexity or not. Besides, it is possible to assign every data to different membership function. Therefore, there is no need to determine the number of membership function in modeling. On the other hand, if the number of the membership function is high, the number of rules will be increased, and there will be the possibility of Meta-learning; consequently, the system will lose its efficiency (Pradhan et al. 2010).

The designed ANFIS model for Firooz Abad-Kojour seismic rockfalls susceptibility mapping with 200 training epochs is shown in Fig. 9. It is worth pointing out that the number of training steps continues where the error-epoch curve becomes horizontal and error reaches a minimum value. In other words, the error reaches a constant value; therefore, increasing the number of training epochs has no effect on reducing the error value. As shown in Fig. 9, error-epoch curve became horizontal after 200 training epochs and the minimum error was 0.024992. Besides, based on the "Subtractive Clustering" method, 12 membership functions were assigned to each input parameter (Fig. 9).

The Firooz Abad-Kojour seismic rockfalls' susceptibility zonation map using ANFIS is shown in Fig. 10. In the ArcGIS software, the seismic rockfalls' susceptibility zonation

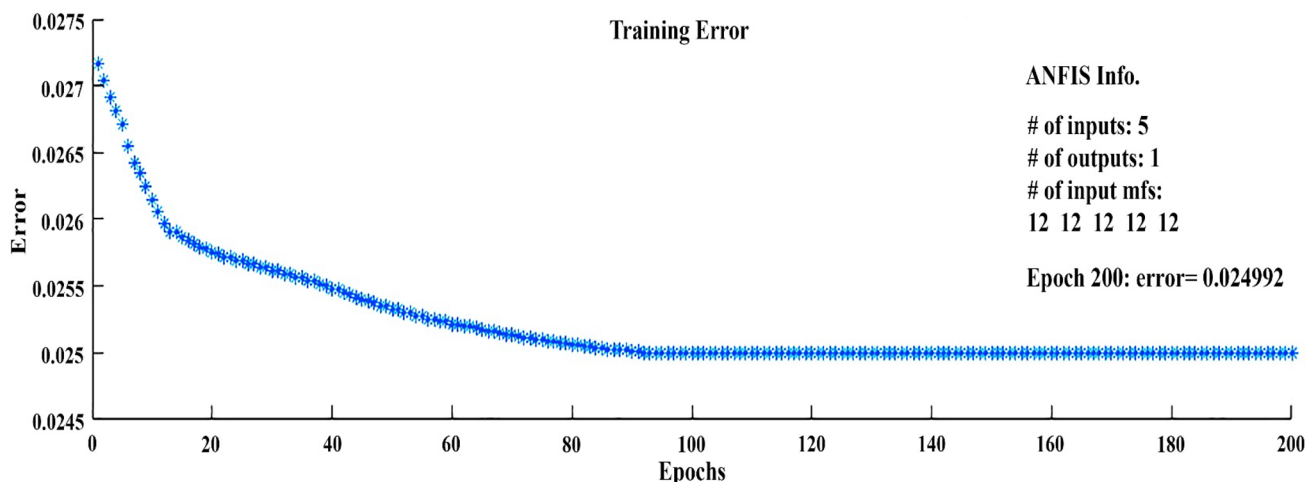


Fig. 9 Error-epoch curve of designed ANFIS model for Firooz Abad-Kojour seismic rockfalls' susceptibility mapping

Hazard zonation map of the Rockfalls induced by the Firooz Abad-Kojour earthquake of 2004 using Adaptive Neuro-Fuzzy Inference System (ANFIS)

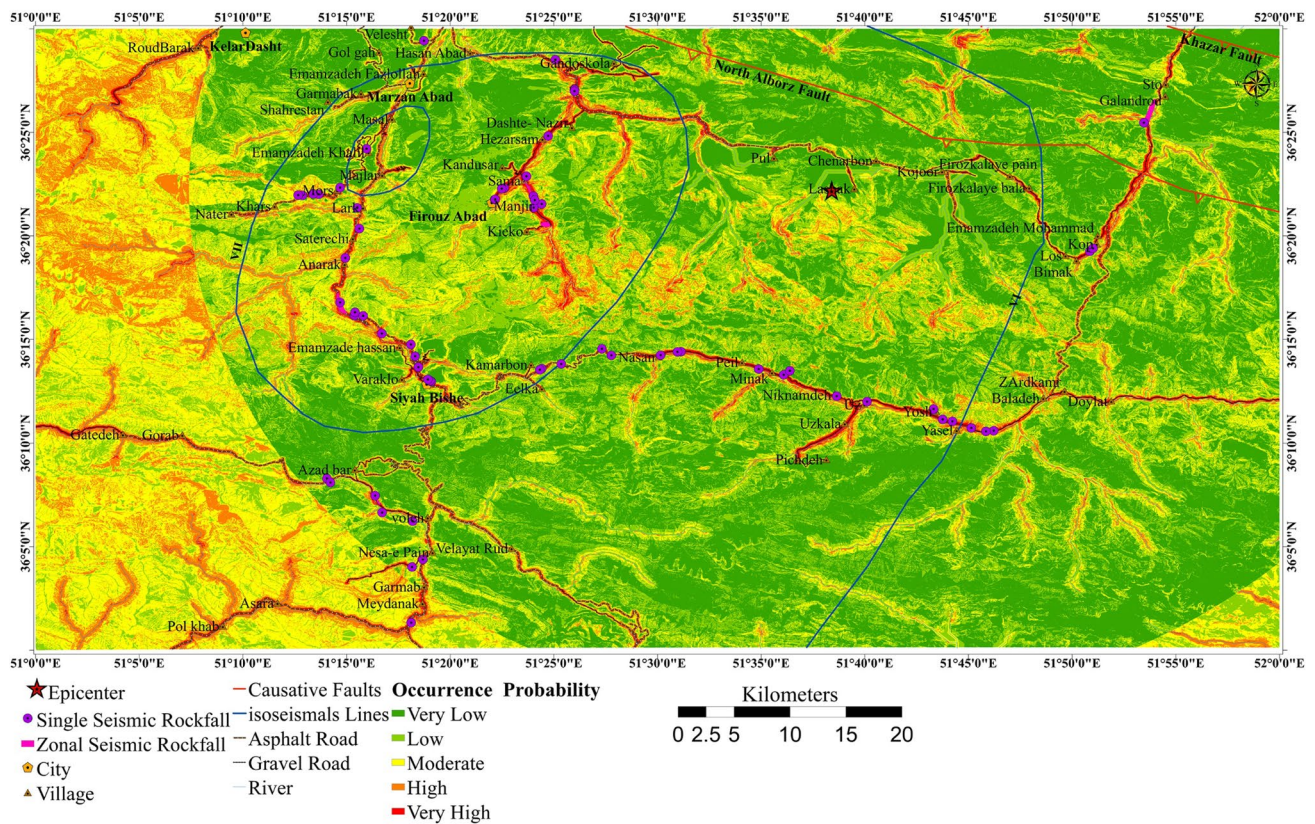


Fig. 10 Hazard zonation map of the rockfalls induced by the Firooz Abad-Kojour earthquake of 2004 using adaptive neuro-fuzzy inference system (ANFIS)

map is classified into five classes of “very low hazard”, “low hazard”, “moderate hazard”, “high hazard”, and “very high hazard” due to the natural breaks (Swets 1988; Bednarik et al. 2010; Constantin et al. 2011; Pourghasemi et al. 2012a, 2013).

As shown in Fig. 10, the share of area susceptible to seismic rockfalls is reduced by increasing the hazard level in the corresponding zones and the majority of rockfalls triggered by Firooz Abad-Kojour earthquake of 2004 are placed at “high hazard”-to-“very high hazard” zones. Besides, the parts close to linking roads, rivers, the parts with a steep slope, the areas around earthquake epicenter, and parts with consisting of low-strength geological formation show a “high”-to-“very high” rockfall susceptibility level. Therefore, it can be concluded the higher and very desirable accuracy of ANFIS model in hazard zonation of rockfalls triggered by the Firooz Abad-Kojour earthquake of 2004.

Since rockfall is a prevalent event in mountainous slopes, coastal cliffs, volcanoes, river margins, and trenches, the rockfalls occur along the rivers and road’s transverse (Wyllie 2014). Since rockfalls mostly occur in cliffs and steep areas, and due to the steep morphology of waterway path and the road’s transverse in mountainous regions, the high

concentrations of rockfalls in the area stricken by Firooz Abad-Kojour earthquake of 2004 seem logical (Fig. 10).

Results’ assessment and analysis

After providing Firooz Abad-Kojour seismic rockfalls’ susceptibility map using the LR and ANFIS methods, and classifying them into five classes based on natural breaks (very low, low, medium, high, and very high susceptibility), their accuracy was evaluated using two introduced indexes by Gee (1992), including density ratio (Dr) and quality sum (Qs), and also, receiver-operating characteristic (ROC) curve.

The dimensionless Dr index was independently used to compare the hazard classes of each map (Eq. 12) (Shariat Jafari 2009):

$$Dr = \frac{\frac{S_i}{A_i}}{\frac{\sum_{i=1}^n S_i}{\sum_{i=1}^n A_i}}, \quad (12)$$

where Dr is falling Dr of each susceptibility class, A_i is area i th susceptibility class in a zonation map, S_i is the sum of

seismic rockfalls in each susceptibility class, A_i is total area of the study region, S_i is the total number of seismic rockfalls in the study area, and n is the number of susceptibility classes. The better separation is performed between susceptibility classes by Dr results in a more useful map. In a given rockfall hazard zonation map, a class with Dr of 1 indicates the moderate hazard probability. Besides, the Dr less and higher than 1 shows the low and high hazard probability, respectively (Shariat Jafari 2009). The values of Dr index for both LR and ANFIS methods are presented in Tables 5 and 6, respectively. As shown in Tables 5 and 6, the Dr index of rockfalls has ascending trend with steep slope from very low to very high hazard class, which indicated the accuracy and good quality of zonation map classification by the LR and ANFIS methods.

To compare the outputs of Firooz Abad-Kojour seismic rockfalls susceptibility models by LR and ANFIS methods, Q_s index was used. The Q_s was calculated for each map by the following equation:

$$Q_s = \sum_{i=1}^n ((Dr - 1)^2 \times \% \text{ area}), \tag{13}$$

where i is hazard class number in a rockfall hazard zonation map, and n is the total number of hazards classes. The Q_s values indicate the performance quality of the model in predicting the hazard of rockfalls in the study area. Typically, there is no theoretical limit to the value of Q_s index (Shariat

Jafari 2009). In other words, the higher Q_s values indicate the optimum model superior in rockfall hazard zonation.

The values of Q_s for Firooz Abad-Kojour seismic rockfall hazard zonation map using both LR and ANFIS methods are presented in Tables 5 and 6, respectively.

The information of Firooz Abad-Kojour seismic rockfalls susceptibility map using the LR is presented in Table 5. The table also shows the area percentage of each rockfall susceptible zone and percentage of seismic rockfalls occurred in each zone. Then, by obtaining those values and applying Eqs. 12 and 13, the Dr of each hazard zone and Q_s of the hazard zonation map prepared using the LR were calculated (Table 5). According to the calculated Dr for each rockfall hazard zone in Table 5, Dr increases ascendingly with an increase in the hazard level. Moreover, the high value of Q_s index (21.04) indicates the proper accuracy of LR method in Firooz Abad-Kojour seismic rockfalls susceptibility mapping.

Table 6 presents the information of Firooz Abad-Kojour seismic rockfalls susceptibility map using the ANFIS. The table also shows the area percentage of each rockfall susceptible zone and percentage of seismic rockfalls occurred in each zone. Then, by obtaining those values and applying Eqs. 12 and 13, the Dr of each hazard zone and Q_s of the hazard zonation map prepared using the ANFIS were calculated (Table 6). According to the calculated Dr for each rockfall hazard zone in Table 6, Dr increases ascendingly with an increase in hazard level. Moreover, the higher value of Q_s (26.75592) indicates the very desirable and acceptable

Table 5 Hazard zonation map information generated using the LR model

| Rockfall hazard zone | Class | Zone area percentage | Occurred rockfall area percentage | Density ratio (Dr) |
|---|-------|----------------------|-----------------------------------|--------------------|
| Very low hazard | 1 | 46.52510511 | 2.702702703 | 0.058091276 |
| low hazard | 2 | 39.71654352 | 10.81081081 | 0.272199186 |
| Moderate hazard | 3 | 10.81421765 | 13.51351351 | 1.249606208 |
| high hazard | 4 | 2.498195049 | 50 | 20.01445004 |
| Very high hazard | 5 | 0.445938669 | 22.97297297 | 51.51599211 |
| Quality sum (Q_s) of the entire map | – | – | – | 21.04184 |

Table 6 Hazard zonation map information generated using ANFIS model

| Rockfall hazard zone | Class | Zone area percentage | Occurred rockfall area percentage | Density ratio (Dr) |
|---|-------|----------------------|-----------------------------------|--------------------|
| Very low hazard | 1 | 36.66769479 | 1.351351351 | 0.036854003 |
| low hazard | 2 | 27.85715286 | 4.054054054 | 0.145530093 |
| Moderate hazard | 3 | 24.50155623 | 9.459459459 | 0.386075863 |
| high hazard | 4 | 9.241885189 | 16.21621622 | 1.754643764 |
| Very high hazard | 5 | 1.73171093 | 68.91891892 | 39.79816592 |
| Quality sum (Q_s) of the entire map | – | – | – | 26.75592 |

accuracy of ANFIS method in Firooz Abad-Kojour seismic rockfall susceptibility mapping.

To evaluate and compare the accuracy of both LR and ANFIS models, ROC curve was used (Yesilnacar 2005; Nefeslioglu et al. 2008; Mathew et al. 2009; Mohammady et al. 2012; Pourghasemi et al. 2012b, c; Pradhan 2013; Regmi et al. 2014). Finally, a map with maximum accuracy was suggested as final Firooz Abad-Kojour seismic rockfalls' susceptibility map.

ROC curve is one of the most important and efficient methods in providing a characteristic, probabilistic identification, and prediction of a system that quantitatively measures the accuracy of the model (Yesilnacar 2005). In ROC curve, the true positive rate (TPR) was drawn against False-Positive Rate (FPR). In the study area, TPR or "sensitivity" and FPR or "specificity", respectively, indicate the probability degree of pixels with and without rockfalls, which were determined correctly by model. The surface under ROC curve, which is known as area under the curve (AUC), shows the model accuracy in predicting the hazard of seismic rockfalls. The ideal model has the highest AUC, which ranges from 0.5 to 1. The qualitative–quantitative correlation of AUC and the estimation evaluation are as follows: 0.9–1 excellent, 0.8–0.9 very good, 0.7–0.8 good, 0.6–0.7 medium, and 0.5–0.6 weak (Yesilnacar 2005). The ROC curve associated with both LR and ANFIS methods, as well as AUC values are presented in Fig. 11.

Based on ROC curve and AUC values (Fig. 11), the AUC for LR and ANFIS methods were calculated 0.972 and 0.984, respectively. Considering the AUC values for LR and ANFIS methods, the ANFIS-based hazard zonation map had higher accuracy compared to LR-based hazard zonation map.

Conclusions and discussion

Given that no research has been conducted on zonation and mapping the susceptibility of seismic rockfalls using intelligent methods (such as ANFIS), the present research was carried out to implement the ANFIS and LR methods in the area stricken by Firooz Abad-Kojour earthquake of 2004, evaluate and select the optimum model with high accuracy in prediction, mapping the susceptibility of seismic rockfalls, and apply this method to predict probability of rockfall events induced by future earthquakes. In LR method, after four steps of analysis, the suitable weights for selected parameters (shake intensity, distance from the road, slope angle, distance from the river, and ground strength class) were obtained based on "backward conditional" rule in SPSS software. Considering the LR-based hazard zonation map, the majority of Firooz Abad-Kojour seismic rockfalls falls in the "high"-to-"very high" hazard zones. Moreover,

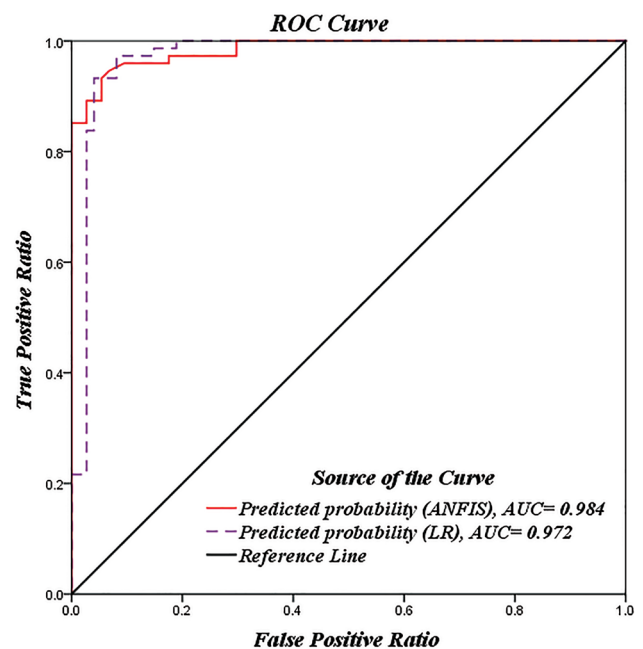


Fig. 11 ROC curve and AUC values associated with Firooz Abad-Kojour seismic rockfall hazard zonation map using the LR and ANFIS methods

the areas close to linking roads, rivers, and low-strength geological formations had "high"-to-"very high" rockfall susceptibility levels. The minimum error of designed ANFIS model for Firooz Abad-Kojour seismic rockfalls susceptibility mapping with 200 training epochs was 0.024992. Considering the ANFIS-based hazard zonation map, the majority of Firooz Abad-Kojour seismic rockfalls was matched on "high"-to-"very high" zones. In addition, the areas close to linking roads, rivers, parts with a steep slope, the area around earthquake epicenter, and low-strength geological formations had "high"-to-"very high" rockfall susceptibility levels.

Rockfalls are very common events that occur in mountainous slopes, coastal cliffs, volcanoes, riverside, and trenches. Since rockfalls mostly occur in cliffs and steep area, and due to the steep morphology of waterway path and road's transverse, we focused on rockfalls in the area stricken by Firooz Abad-Kojour earthquake of 2004.

After preparing the Firooz Abad-Kojour seismic rockfalls susceptibility map using LR and ANFIS methods, criteria including D_r , Q_s , and ROC were used to evaluate the considered map and determine its accuracy. The D_r of rockfalls had an ascending trend with high slope from "very low" to "very high" hazard class, suggesting the good quality and accuracy of LR and ANFIS-based hazard zonation maps. By analyzing the susceptibility maps and considering the Q_s index obtained by LR (21.04184) and ANFIS (26.75592), it could be observed that the Q_s value of ANFIS is higher

than that of LR. Moreover, based on the obtained value of AUC from LR (0.972) and ANFIS (0.984) methods, ANFIS provided a higher accuracy in zonation and susceptibility mapping of rockfalls triggered by Firooz Abad-Kojour earthquake of 2004 compared to LR method. Therefore, based on the verification done using the criteria such as “Dr” and “Qs”, and ROC curve, ANFIS-based Firooz Abad-Kojour seismic rockfalls susceptibility mapping was in agreement with the rockfall distribution map of the area and showed a higher accuracy compared to LR method.

Performing an analysis on the effect of geomechanical properties of geological material on probability of rockfall event, the generalization of this approach for synergetic seismic and hydrological activities (such as snow melting and rainfall), and evaluating the accuracy of ANFIS model in comparison with artificial neural network (such as MLP and RBF) are recommended for future research.

References

- Agliardi F, Crosta GB, Frattini P (2009) Integrating rockfall risk assessment and countermeasure design by 3D modeling techniques. *Nat Hazards Earth Sys Sci* 9(4):1059
- Amini Hosseini K, Mahdavi MR, Bakhshayesh MK, Khazaie B, Azadi A, Bidar AS, Ravanfar SO, Kamalpour F, Rakhshandeh M, Banki Sh (2004) Earthquake-induced Landslide Identification Report of the 2004/05/28 Firuzabad (Kojur) earthquake. *Seismol Earthq Eng Res J Int Inst Seismol Earthq Eng* 7(2):21–36 (in Persian)
- Arias A (1970) A measure of the earthquake intensity in seismic design for nuclear power plants. Massachusetts Institute of Tech Press, Cambridge, pp 438–468
- Ayalew L, Yamagishi H (2005) The application of GIS-based logistic regression for landslide susceptibility mapping in the Kakuda-Yahiko Mountains, Central Japan. *Geomorph J* 65(1):15–31
- Bednarik M, Magulová B, Matys M, Marschalko M (2010) Landslide susceptibility assessment of the Kraľovany–Liptovský Mikuláš railway case study. *Phys Chem Earth Parts A/B/C* 35(3):162–171
- Budimir MEA, Atkinson PM, Lewis HG (2015) A systematic review of landslide probability mapping using logistic regression. *Landslide J* 12(3):419–436
- Bui DT, Pradhan B, Lofman O, Revhaug I, Dick OB (2012) Spatial prediction of landslide hazards in Hoa Binh province (Vietnam): a comparative assessment of the efficacy of evidential belief functions and fuzzy logic models. *Catena* 96:28–40
- Cancelli A, Crosta G (1993) Rockfall hazard, and risk mapping. In: *Proceedings 7th international conference and field workshop on landslides, Czech-Slovak Rep., Balkema*, pp 69–76
- Capolongo D, Refice A, Mankelov J (2002) Evaluating earthquake-triggered landslide hazard at the basin scale through GIS in the Upper Sele river valley. *Surv Geophys* 23(6):595–625
- Chau KT, Wong RHC, Liu J, Lee CF (2003) Rockfall hazard analysis for Hong Kong based on rockfall inventory. *Rock Mech Rock Eng* 36(5):383–408
- Chauhan S, Sharma M, Arora MK (2010) Landslide susceptibility zonation of the Chamoli region, Garhwal Himalayas, using logistic regression model. *Landslide J* 7(4):411–423
- Constantin M, Bednarik M, Jurchescu MC, Vlaicu M (2011) Landslide susceptibility assessment using the bivariate statistical analysis and the index of entropy in the Sibiciu Basin (Romania). *Environ Earth Sci* 63(2):397–406
- Corominas J, Copons R, Moya J, Vilaplana JM, Altimir J, Amigó J (2005) Quantitative assessment of the residual risk in a rockfall protected area. *Landslide J* 2(4):343–357
- Corominas J, Mavrouli O, Ruiz-Carulla R (2017) Rockfall Occurrence and Fragmentation. In *Workshop on World Landslide Forum*. Springer, 75–97
- Cox DR (1958) The regression analysis of binary sequences. *J R Stat Soc Ser B (Methodol)* 20(2):215–242
- Dashti Marvily M (2008) Landslide hazard zoning using logistic regression (case study: a part of gamasiab watershed). M.Sc Thesis. Tarbiat Modares University, pp 92 (in Persian)
- Del Gaudio V, Wasowski J (2004) Time probabilistic evaluation of seismically induced landslide hazard in Irpinia (Southern Italy). *Soil Dyn Earthq Eng* 24(12):915–928
- Del Gaudio V, Pierri P, Wasowski J (2003) An approach to the time-probabilistic evaluation of seismically induced landslide hazard. *Bull Seismol Soc Am* 93(2):557–569
- Ercanoglu M, Gokceoglu C (2002) Assessment of landslide susceptibility for a landslide-prone area (north of Yenice, NW Turkey) by the fuzzy approach. *Environ Geo* 41:720–730
- Fatemi Aghda SM, Bagheri V (2015) Evaluation of earthquake-induced landslides hazard zonation methods: a case study of Sarein, Iran, earthquake (1997). *Arabian J Geosci* 8(9):7207–7227
- Garsia-Rodríguez MJ, Malpica JA, Benito B, Díaz M (2008) Susceptibility assessment of earthquake-triggered landslides in El Salvador using logistic regression. *Geomorph J* 95(3):172–191
- Gee MD (1992) Classification of landslide hazard zonation methods and a test of predictive capability. In: *Proceedings of 6th international symposium on landslides, Christchurch, New Zealand, vol 2*, pp 947–952
- Gosar A (2017) Earthquake-induced rockfalls caused by 1998 Mw5. 6 earthquake in Krn mountains (NW Slovenia) and ESI 2007 Intensity Scale. In: *Workshop on world landslide forum*. Springer, pp 131–139
- Hung O, Evans SG, Hazzard J (1999) Magnitude and frequency of rock falls and rock slides along the main transportation corridors of southwestern British Columbia. *Can Geotech J* 36(2):224–238
- Jaboyedoff M, Dudd JP, Labiouse V (2005) An attempt to refine rockfall hazard zoning based on the kinetic energy, frequency and fragmentation degree. *Nat Hazards Earth System Sci* 5(5):621–632
- Jang JS (1993) ANFIS: adaptive-network-based fuzzy inference system. *IEEE Trans Syst Man Cybern* 23(3):665–685
- Jibson RW, Harp EL, Michael JA (2000) A method for producing digital probabilistic seismic landslide hazard maps. *Eng Geol* 58(3):271–289
- Keefer DK (1984) Landslides caused by earthquakes. *Geol Soc Am Bull* 95(4):406–421
- Keefer DK (2000) Statistical analysis of an earthquake-induced landslide distribution -the 1989 Loma Prieta, California event. *Eng Geol J* 58:231–249
- Lari S, Frattini P, Crosta GB (2014) A probabilistic approach for landslide hazard analysis. *Eng Geol* 182:3–14
- Lee S, Sambath T (2006) Landslide susceptibility mapping in the Damrei Romel area, Cambodia using frequency ratio and logistic regression models. *Environ Geol* 50(6):847–855
- Lee CT, Huang CC, Lee JF, Pan KL, Lin ML, Dong JJ (2008) Statistical approach to earthquake-induced landslide susceptibility. *Eng Geol* 100(1):43–58
- Mahdavi MR (2006) Analytical evaluation and design of the system (GIS) for seismic landslides hazard management in Iran. Ph.D. thesis. In: *International Institute of Earthquake Engineering and Seismology*, pp 213 (in Persian)
- Mahdavi MR, Jafari MK, Zolfaghari MR (2007) The attenuation of Arias intensity in Alborz and Central Iran. In: *The fifth*

- international conference on seismology and earthquake engineering, Tehran, Iran: pp 7
- MahdaviFar M, Askari F, Memarian P, Seyedimorad SM (2016) Earthquake-induced rock fall hazard zonation of Varzegha-Ahar region in northwest Iran: a comparison of quantitative and qualitative approaches. *J Seismol Earthq Eng* 18(2):101–116
- Marzorati S, Luzi L, De Amicis M (2002) Rock falls induced by earthquakes: a statistical approach. *Soil Dyn Earthq Eng J* 22(7):565–577
- Massey CI, MacSaveney MJ, Richards L (2015) Characteristics of some rockfalls triggered by the 2010/2011 Canterbury earthquake sequence, New Zealand. In: *Eng Geo for Soci and Terri*, Springer, vol 2, pp 1943–1948
- Mathew J, Jha VK, Rawat GS (2009) Landslide susceptibility zonation mapping and its validation in part of Garhwal Lesser Himalaya, India, using binary logistic regression analysis and receiver operating characteristic curve method. *Landslide J* 6(1):17–26
- Miles SB, Keefer DK (2007) Comprehensive areal model of earthquake-induced landslides: Technical specification and user guide. U.S. Geological Survey Open-File Report 2007–1072: pp 69
- Miles SB, Keefer DK (2009a) Evaluation of CAMEL—comprehensive areal model of earthquake-induced landslides. *Eng Geol* 104(1):1–15
- Miles SB, Keefer DK (2009b) Toward a comprehensive areal model of earthquake-induced landslides. *Nat Hazards Rev* 10(1):19–28
- Mohammady M, Pourghasemi HR, Pradhan B (2012) Landslide susceptibility mapping at Golestan Province, Iran: a comparison between frequency ratio, Dempster–Shafer, and weights-of-evidence models. *J Asian Earth Sci* 61:221–236
- Motamedi M, Liang RY (2013) Probabilistic landslide hazard assessment using Copula modeling technique. *Landslide J* 11(4):565–573
- Nefeslioglu HA, Gokceoglu C, Sonmez H (2008) An assessment of the use of logistic regression and artificial neural networks with different sampling strategies for the preparation of landslide susceptibility maps. *Eng Geol* 97(3):171–191
- Oh HJ, Pradhan B (2011) Application of a neuro-fuzzy model to landslide susceptibility mapping for shallow landslides in a tropical hilly area. *Comp Geosci* 37(9):1264–1276
- Peng WF, Wang CL, Chen ST, Lee ST (2009) Incorporating the effects of topographic amplification and sliding areas in the modeling of earthquake-induced landslide hazards, using the cumulative displacement method. *Comp Geosci* 35(5):946–966
- Petley DN (2012) Landslides and engineered slopes: protecting society through improved understanding. *Landslide Eng Slopes J* 1:3–13
- Polat K, Güneş S (2006) Hepatitis disease diagnosis using a new hybrid system based on feature selection (FS) and artificial immune recognition system with fuzzy resource allocation. *Digital Signal Proces* 16(6):889–901
- Pourghasemi HR, Mohammady M, Pradhan B (2012a) Landslide susceptibility mapping using the index of entropy and conditional probability models in GIS: Safarood Basin, Iran. *Catena J* 97:71–84
- Pourghasemi HR, Pradhan B, Gokceoglu C, Moezzi KD (2012b) Landslide susceptibility mapping using a spatial multi-criteria evaluation model at Haraz Watershed, Iran. In: *Terrigenous mass movements*. Springer, Berlin, pp 23–49
- Pourghasemi HR, Pradhan B, Gokceoglu C (2012c) Application of fuzzy logic and analytical hierarchy process (AHP) to landslide susceptibility mapping at Haraz watershed, Iran. *Nat Hazards* 63(2):965–996
- Pourghasemi H, Pradhan B, Gokceoglu C, Moezzi KD. *Geomatics* (2013) A comparative assessment of prediction capabilities of Dempster–Shafer and weights-of-evidence models in landslide susceptibility mapping using GIS. *Nat Hazards Risk* 4(2):93–118
- Pradhan B (2013) A comparative study on the predictive ability of the decision tree, support vector machine and neuro-fuzzy models in landslide susceptibility mapping using GIS. *Comp Geosci* 51:350–365
- Pradhan B, Sezer EA, Gokceoglu C, Buchroithner MF (2010) Landslide susceptibility mapping by the neuro-fuzzy approach in a landslide-prone area (Cameron Highlands, Malaysia). *IEEE Trans Geosci Remote Sens* 48(12):4164–4177
- Rapolla A, Paoletti V, Secomandi M (2010) Seismically-induced landslide susceptibility evaluation: application of a new procedure to the island of Ischia, Campania Region, Southern Italy. *Eng Geol* 114(1):10–25
- Regmi NR, Giardino JR, McDonald EV, Vitek JD (2014) A comparison of logistic regression-based models of susceptibility to landslides in western Colorado, USA. *Landslide J* 11(2):247–262
- Rodríguez CE, Bommer JJ, Chandler RJ (1999) Earthquake-induced landslides: 1980–1997. *Soil Dyn Earthq Eng J* 18(5):325–346
- Shariat Jafari M (2009) Specific risk zonation of landslides in the critical (Central Alborz) zones. National Disaster Mitigation Organization. A specialized workshop of earthquake and landslide, pp 95 (in Persian)
- Straub D, Schubert M (2008) Modeling and managing uncertainties in rock-fall hazards. *Georisk* 2(1):1–15
- Sugeno M (1985) *Industrial applications of fuzzy control*. Elsevier Science Ltd., Amsterdam, pp 278
- Swets JA (1988) Measuring the accuracy of diagnostic systems. *Science* 240(4857):1285–1293
- Turner AK, Jayaprakash GP (2012) Introduction. In: Turner AK, Schuster RL (eds) *Rockfall characterization and control*. Transportation Research Board, National Academy of Sciences, Washington, DC, pp 3–20
- Uchida T, Osanai N, Onoda S, Takayama T, Tomura K (2006) A simple method for producing probabilistic seismic shallow landslide hazard maps. In: *Proceedings of interpraevent*, Universal Academy Press, vol 2, pp 529–534
- Valagussa A, Frattini P, Crosta GB (2014a) Quantitative probabilistic hazard analysis of earthquake-induced rockfalls. In: *Landslide science for a safer geoenvironment*, Springer, pp 213–218
- Valagussa A, Frattini P, Crosta GB (2014b) Earthquake-induced rockfall hazard zoning. *Eng Geol* 182:213–225
- Varnes DJ (1978) Slope movement types and processes. *Special report* 176:11–33
- Wang YM, Elhag TM (2008) An adaptive neuro-fuzzy inference system for bridge risk assessment. *Expert Syst Appl* 34(4):3099–3106
- Wasowski J, Del Gaudio V (2000) Evaluating seismically induced mass movement hazard in Caramanico Terme (Italy). *Eng Geol* 58(3):291–311
- Wilson RC (1993) Relation of Arias Intensity to Magnitude and Distance in California. U.S Geological Survey Open-File report 1993-556, pp 41
- Wyllie DC (2014) *Rock fall engineering*. CRC Press, Baco Raton, pp 270
- Yesilnacar EK (2005) *The Application of Computational Intelligence to Landslide Susceptibility Mapping in Turkey*, Ph.D. Thesis. Department of Geomatics the University of Melbourne: pp 423
- Yilmaz I (2009) Landslide susceptibility mapping using frequency ratio, logistic regression, artificial neural networks and their comparison: a case study from Kat landslides (Tokat—Turkey). *Comp Geosci* 35(6):1125–1138
- Yin KL, Yan TZ (1988) Statistical prediction model for slope instability of metamorphosed rocks. In: *Proceedings of the 5th*

- international symposium on landslides, Lausanne, Switzerland, AA Balkema Rotterdam, The Netherlands. vol 2, pp 1269–1272
- Ying LC, Pan MC (2008) Using adaptive network-based fuzzy inference system to forecast regional electricity loads. *Energy Convers Manag* 49(2):205–211
- Zare M (2004) Seismology and earthquake engineering aspects of the 2004/05/28 Firuzabad (Kojur) earthquake with magnitudes $M_w = 6.2$. *Seismol Earthq Eng Res J Int Inst Seismol Earthq Eng* 7(2):45–57 (**in Persian**)

Publisher's Note Springer Nature remains neutral with regard to jurisdictional claims in published maps and institutional affiliations.